Energy Conversion and Management: X 19 (2023) 100402

Contents lists available at ScienceDirect

Energy Conversion and Management: X

journal homepage: www.sciencedirect.com/journal/energy-conversion-and-management-x

Analysis of a solar driven ORC-absorption based CCHP system from a novel exergy approach

Jesús García-Domínguez [a,*], Ana M. Blanco-Marigorta [b], J. Daniel Marcos [a]

[a] Universidad Nacional de Educación a Distancia, UNED, E.T.S. Ingenieros Industriales, Departamento de Ingeniería Energética, C/ Juan del Rosal 12, 28040 Madrid, Spain

[b] Universidad de Las Palmas de Gran Canaria, Departamento de Ingeniería de Procesos, Edificio de Ingenierías-Tafira Baja, 35017 Las Palmas, G.C., Spain

ARTICLE INFO

Keywords:
Organic Rankine Cycle
Trigeneration
Solar thermal energy
Exergy
Novel approach

ABSTRACT

The present study comprehensively analyses the thermodynamic performance of a zero-emissions solar driven trigeneration system using a numerical approach. The analysis is conducted from both the First and Second law of Thermodynamics viewpoints, employing a novel and coherent exergy approach. Solar parabolic trough collectors (SPTCs) provide the heat input to an organic Rankine cycle (ORC) system, while a single-effect H_2O/LiBr absorption heat pump is coupled in cascade to the ORC. The proposed ORC layout is based on a single-pressure regenerated, recuperated and superheated cycle. There is divergence of opinion among researchers regarding key aspects of the exergy analysis of trigeneration systems. Therefore, this study proposes the definition of the dead state conditions for each subsystem individually, taking into account their specific constraints. Unlike temperature, specific dead state conditions for pressure and composition are defined separately. An energy-exergy parametric approach is conducted to evaluate the effects of different system parameters on the system performance. The system is also optimized following single and multi-objective approaches with different criteria. The optimum system achieve an energy efficiency of 152.4%, an exergy efficiency of 21.1%, and an electrical-exergy efficiency of 17.5%. The electricity, cooling and heating productions are 82.1 kW, 200.4 kW and 471.7 kW, respectively. The SPTCs are identified as the main source of exergy destruction, responsible for 73% of inlet exergy is destructed. In addition, the systems performance is shown to be sensitive to the variations in the solar field outlet temperature and in the ORC condensation temperature. Consequently, controlling these parameters could be effectively utilized for regulating power generation as well as cooling and heating production.

Introduction

The use of Organic Rankine Cycle (ORC) as a prime mover of a trigeneration thermal system is a promising alternative to produce cooling, heating, and power simultaneously from the same energy source [1]. Based on the market review provided by Wieland et al [2], the cumulated ORC installed capacity to date exceeds 4 GW. There are several studies focused on the technical and economic evaluation for power generation with ORC that conclude that this is a viable and mature technology to convert low-medium temperature heat into electricity. Colona et al. [3] consider that ORC systems are suitable for distributed cogeneration applications. The use of waste heat and renewable energy as heat source of ORC technology has enormous potential for power generation and heating/cooling applications [4]. Unlike steam cycle, ORC systems are better suited for moderate power ranges applications [5].

Careful selection of cycle layout and working fluid are key criteria for optimizing an ORC. Lecompte et al [6] carried out a literature review focused on cycle configurations. Branchini et al. [7] compared different arrangements of the ORC system and different working fluids following a parametric analysis, concluding that both the evaporation pressure and the heat source temperature are key parameters in power cycle performance and in the selection of the best ORC configuration. Li et al. [8] assessed and compared single-pressure and dual-pressure evaporation ORCs using pure working fluids with heat source temperatures ranging 100–200 °C and without restriction on the outlet evaporator temperature; the results showed that for a heat source temperature above a certain value, the ORC with a dual-pressure evaporator offers no advantage. Wang et al. [9] determined that some key thermodynamic design parameters like turbine inlet pressure and temperature, pinch and approach temperature difference in the heat recovery vapor

* Corresponding author at: The International Doctoral School of UNED, Industrial Technologies, Spain.
E-mail address: jgarcia5088@alumno.uned.es (J. García-Domínguez).

https://doi.org/10.1016/j.ecmx.2023.100402
Received 23 January 2023; Received in revised form 29 May 2023; Accepted 1 June 2023
Available online 7 June 2023

Nomenclature

Symbols

h	*heat transfer coefficient, W/(m2 K)*
$\dot{m}$	*mass flow rate, kg/s*
T	*temperature, °C*
ΔT	*temperature difference, °C*
s	*entropy, kJ/kg K*
η	*efficiency*
$\dot{W}$	*electric power, kW*
$\dot{Q}$	*thermal power, kW*
$\dot{q}'$	*heat rate per SPTC unit length, kW/m*
$\dot{E}x$	*exergy, kW*
$\dot{ex}$	*specific exergy, kJ/kg*
w_{ap}	*aperture width of SPTC, m*
L	*length of SPTC, m*
N	*number of SPTCs*
θ	*solar incidence angle on the SPTC,*
X	*mass fraction*
μ	*chemical potential, kJ/kg*
Y	*exergy destruction ratio*
Y^*	*irreversibility ratio*

Acronyms

CCHP	combined cooling heating and power
ORC	organic Rankine cycle
SPTC	solar parabolic trough collector
SH	superheater heat exchanger or superheated cycle
EVA	evaporator heat exchanger
ECO	economizer heat exchanger
DNI	direct normal irradiance
LS	live steam
PP	pinch point
AP	approach point
COP	coefficient of performance
UA	overall heat transfer coefficient
LMTD	log mean temperature difference
HX	heat exchanger

Subscripts

en	energy
ex	exergy
el	electricity
sol	solar field
0	dead conditions
in	inlet
out	inlet
turb	turbine
cond	heat conduction
conv	heat convection
rad	heat radiation
SolAbs	solar absorption
hp	heat pump
e	evaporator of the heat pump
c	condenser of the heat pump
d	desorber of the heat pump
tri	trigeneration
s.he	solution heat exchanger
s.pump	solution pump
cool	heat-pump cooling mode
heat	heat-pump heating mode
ph	physical
ch	chemical
k	component
z	subsystems
i	substance
j	state
P	product
F	fuel
D	destruction
L	loss
Tot	total

generator, and the working fluid, have an influence on the net power output and surface areas of the heat exchangers.

Numerous works in the literature investigated the selection of organic fluids based on thermodynamic, technical, and economic performance criteria. Wet fluids are not suitable for ORC applications due to larger vaporizing enthalpy [10,11]. On the contrary, isentropic fluids are the best working fluids candidates for ORC systems [11]. Rayegan and Tao [12] developed a procedure to compare capabilities of working fluids in solar driven regenerative ORCs; they selected eleven fluids as good candidates for low-medium temperature solar ORC applications. Following an analysis of internal and external exergy efficiencies of ORC systems, Long et al [13] concluded that the selection of working fluids depends greatly on the optimal evaporation temperature. In terms of fluid composition, Zeotropic mixtures normally present higher efficiencies than pure fluids due to better glide matching of temperature in the evaporation process [14].

The most typical heat sources of an ORC are either waste heat, solar energy, geothermal heat or biomass combustion [6,15]. Different temperature ranges can be used to categorize sources, from the limit values (100–300 °C) for geothermal and solar applications, up to values of 400–600 °C related to topping power systems (such as gas turbines, steam Rankine cycle and reciprocating engines). Specifically for solar-driven ORC applications, Loni et al. [16] recently presented a complete review on the use of a wide range of different solar collectors to be coupled to ORC systems; the authors concluded that SPTCs are one of the most effective technologies presenting an overall system efficiency above 20%. The combination of solar driven ORC power cycles with combined cooling and heating applications based on absorption technology, the so called solar driven ORC-absorption based CCHP, have recently been under investigation [17,18]. Numerous studies were conducted recently to evaluate the thermal and financial performance of various system configurations. Suleman et al. [19] analysed a novel integrated solar and geothermal energy system with two ORCs for power generation and an absorption chiller for cooling production. The overall energy efficiency was estimated at 54.7%. Concerning net zero energy building applications, Hassoun and Dincer [20] proposed a multigenerational system reporting an overall system exergy efficiency of 44.7%. A trigeneration system powered by SPTCs was evaluated by Al-Sulaiman et al. [21] to generate 500 kW of electricity through an ORC system. The findings revealed that the CCHP's overall energy efficiency was 94%, while the electrical efficiency was 15%. Bellos and Tzivanidis [22] investigated a solar-powered CCHP system using parametric optimization for various working fluids and design parameters. In the best-case scenario, electric exergy and energy efficiency ratios found were 27.9% and 22.5%, respectively, while energy performance ranged from 130% to 180%. The CCHP layout configuration is an important factor on the system efficiency. García-Domínguez and Marcos [23] compared six alternative solar heated ORC-absorption based CCHP configurations derived from single-pressure and dual-pressure ORC layouts with different organic fluids. The results indicated that for a heat source ranging 180–240 °C the dual-pressure evaporation ORC is unbefitting, and the most efficient layout is the single-pressure regenerative

recuperated superheated ORC with toluene as working fluid; the overall energy and exergy efficiency found were 163.7% and 12.3%, respectively.

Although numerous investigations have been conducted on the energy analysis and performance evaluation of solar driven ORC-absorption based CCHP from the first law viewpoint, very limited reviewed papers in the literature have appeared on detailed exergy analysis and performance assessment of such systems. Al-Sulaiman et al. [24] assessed the exergetic performance of a solar driven ORC-absorption based CCHP system under three modes of operation (solar, solar and storage, and storage). For a SPTCs outlet temperature of 600 K and an ORC condensing temperature of 365 K, the maximum trigeneration-exergy efficiency for the best operating mode was 20%. Karellas and Braimakis [25] analysed a micro-scale CCHP system based on the combined operation of an ORC and a Vapor Compression Cycle (VCC) utilizing biomass fuel and solar power. The maximum electrical-exergy efficiency for an ORC evaporator temperature of 159 °C was estimated at 7.5%. Eisavi et al. [26] conducted a thermodynamic analysis of an ORC based CCHP system with SPTCs as a heat source and a double effect H_2O/ LiBr absorption chiller to produce cooling power. For a solar source outlet temperature of 327 °C and an ORC condensing temperature of 120 °C, the exergy efficiency ratios for electricity, heating-cogeneration, and cooling-cogeneration were 4.4%, 12.8%, and 4.5%, respectively. A novel solar trigeneration energy system consisting of a heliostat field, ORC and an ejector-absorption chiller is introduced and analysed by Khaliq et al. [27]. The maximum trigeneration-exergy efficiency found is about 14%. A new solar-based CCHP involving SPTCs, ORC, two heating processes, and two single-effect absorption chillers was developed and investigated by Haghghi et al. [28]. For a pure solar mode, the overall energy and exergy efficiency found are 98% and 17%, respectively. Two solar powered trigeneration systems based on different ORC configurations and double-effect absorption chiller were analysed and compared from energetic and exergetic viewpoints by Jafary et al. [29]. The results revealed that the overall exergy efficiency for the best configuration was 12.7%. Aghaziarati and Aghdam [30] proposed and investigated a novel solar ORC integrated cascade refrigeration system including both a vapor absorption and a vapor compression refrigeration system to meet heating, cooling and electricity demands for a hospital. The energy and exergy efficiency ratios of the CCHP system found were 89.4% and 8.70%, respectively.

The cited studies reveal a disparity on methodologies and hypothesis considered for the calculation of the exergy streams, for the dead state definition, and for the definition of the exergy efficiency of the different components. The selection of the dead state conditions in the above-mentioned references follows the common approach to set the environmental pressure and temperature as dead state condition (i.e., ambient pressure 100 kPa, ambient temperature 15–25 °C); however, the choice of a suitable dead state is important in the exergy calculation and deserves special attention. Exergy is defined as the maximum amount of work that a flow or system can produce in a given environment or relative to a dead state. The greater the difference between the energy source of a system and its environment, the greater the capacity to extract work from the system. Rosen and Dincer [31] proved that although the energy and exergy values depend on the dead state conditions, the main results of energy and exergy analyses are usually not significantly sensitive to reasonable variations in these properties when the state of the system is significantly different from that of the selected dead state. On the other hand, Blanco-Marigorta and Marcos [32] with a new approach for the exergy analysis of H_2O/LiBr absorption cooling systems confirmed certain discrepancy in the exergy results for some components of an absorption heat pump with respect to other authors following different methodologies. They proved that the choice of the ambient pressure as the dead state condition for closed refrigeration cycles does not seem logical.

None the cited papers consider the calculation of the chemical exergy of the streams in the analysis; however, in the solution side of the H_2O/LiBr absorption heat pump there are changes in the composition of the fluid, so the chemical exergy must be considered in the exergy balances of some components. Another discrepancy is how the results of the exergy analysis are presented for the overall system and for each component separately. The abovementioned cited articles use the so-called rational efficiency which relates exergetic gain (fuel exergy) to exergetic expenditure (product exergy) [33,34]. However, some authors are just interested either in the overall exergy efficiency or in the overall exergy destruction [24,28,29]. A specific exergy analysis at the component level is carried out by other authors, but they only provide the exergy destruction or losses [26,27]. The exergy efficiency of each device of the system is analysed by Refs. [25,30].

The main objective of the present study is to conduct a detailed thermodynamic analysis of solar heated ORC-absorption based CCHP system using a novel exergy approach. The evaluated CCHP system primarily consists of a regenerative recuperated and superheated ORC layout for power generation driven by SPTCs. A single-effect H_2O/LiBr absorption heat-pump is coupled in cascade to the ORC as a bottoming cycle to simultaneously fulfil heating and cooling demands. The exergy analysis performed in this study focuses on defining the dead state conditions and calculating the exergy stream for each subsystem individually, i.e., solar field, ORC, and absorption heat pump. The proposed methodology considers that the working fluids are confined in each subsystem, meaning they are not in mechanical or chemical equilibrium with the environment. Therefore, only thermal equilibrium can be reached in the dead state. Consequently, assuming that the dead-state pressure is equal to atmospheric pressure is not valid.

The novelty of this study can be summarised as follows:

a) the utilization of an ORC cycle arrangement as a prime mover for a solar driven CCHP to maximise the overall efficiency, that is, a single-pressure ORC regenerative recuperated superheated cycle,
b) the definition of the dead state for each subsystem of the CCHP system individually, taking into account their unique constraints, and
c) the definition and calculation of the exergy of the material streams and the exergy efficiency of each component within the CCHP, including both individual components and the overall system.

Description of the system and assumptions

The trigeneration system evaluated in this study is presented in Fig. 1. It mainly consists of three subsystems which are thermally connected: (i) an ORC for power generation, states 1–11, which is driven by a solar field of parabolic trough collectors (ii), states $\acute{1}-\acute{4}$, and finally a single-effect H_2O/LiBr absorption heat pump (iii), states $\acute{1}-\acute{16}$, which is integrated as a bottoming cycle to meet heating and cooling demands simultaneously.

Organic Rankine cycle

In addition to the input from solar model, which is the outlet temperature of the solar field, the selection of the ORC layout is key on the overall performance of the CCHP system. Among the different possible cycle configurations, the regenerative recuperated superheated ORC is selected. According to [23] the proposed ORC configuration is 16% more efficient than the simple cycle.

The evaporator is the element that connects the heat source supplied by the SPTCs and the ORC. The layout selected for the single-pressure evaporator consists of three elements: i) economiser, where the working fluid is heated up to the fluid evaporation temperature minus the approach point (AP); ii) evaporator, where the evaporation process is produced at constant temperature and pressure; and iii) superheater, where the saturated steam is heated above the evaporation temperature up to the outlet temperature of the live steam (T_{LS}). The design parameters for the ORC model are given in Table 1. One of the key

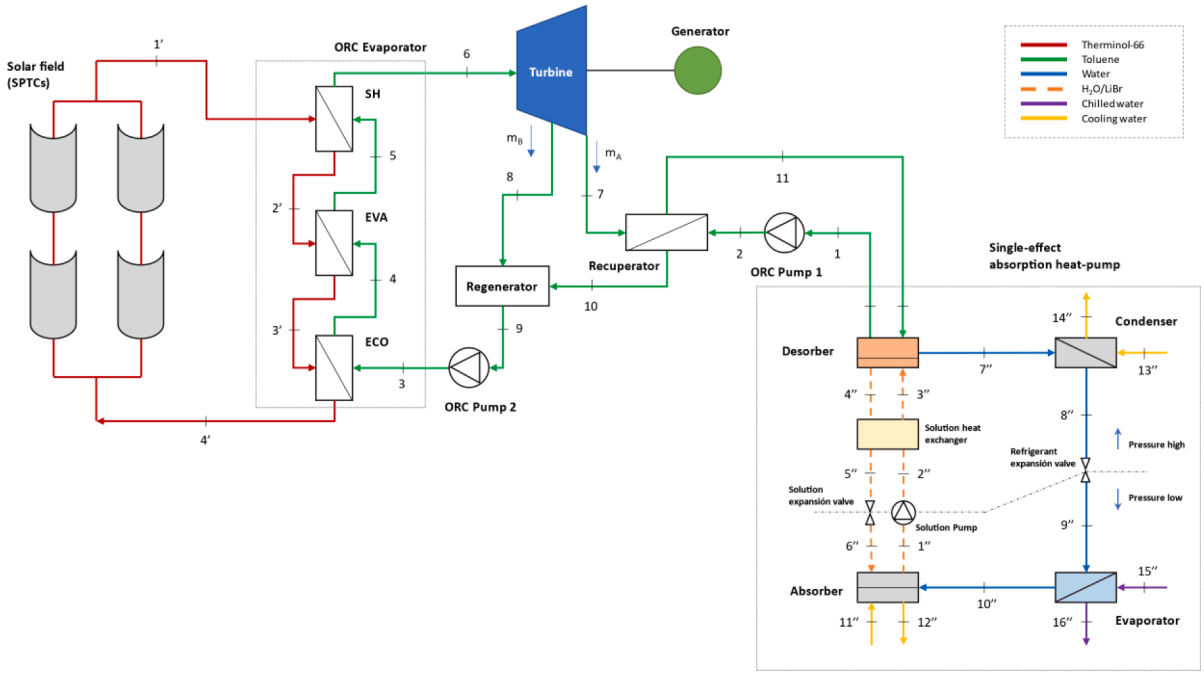

Fig. 1. CCHP with ORC Regenerative recuperated superheated cycle.

Table 1
Input data for ORC model [21,34].

Parameter	Value
Condensation temperature (T_1)	90 °C
Turbine isentropic efficiency (η_{turb})	85%
ORC pump isentropic efficiency ($\eta_{ORC,pump}$)	70%
Recuperator efficiency (η_{REC})	70%
Superheating (ΔT_{SH})	10 °C
Live steam outlet temperature (T_{LS})	$T_{\dot{I}}$ - (35 - ΔT_{SH})
Pinch Point (PP)	7 K
Approach Point (AP)	5 K

parameters that is examined in the parametric analysis is the ORC condensing temperature; the rest of the chosen parameters are coherent with possible thermophysical constraints of the different heat exchangers of the system. Fig. 2 represents the correspondent heat transfer–temperature diagrams for the complete evaporator and Fig. 3 the T-s diagram for the proposed ORC configuration.

On the other hand, it is crucial to choose a suitable working fluid that maximizes the efficiency of the ORC, but at the same time is a chemically stable fluid in the chosen working temperature range. The environment

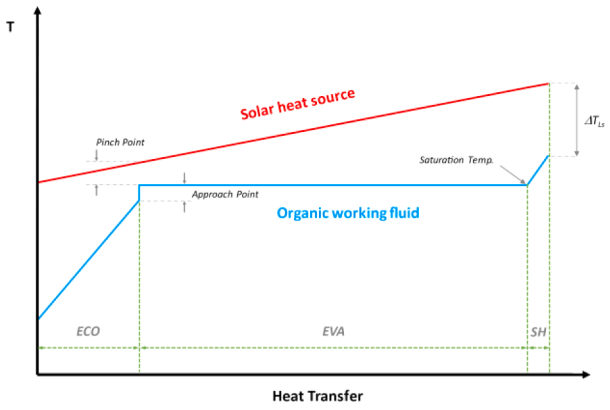

Fig. 2. Heat transfer-temperature diagram in the evaporator.

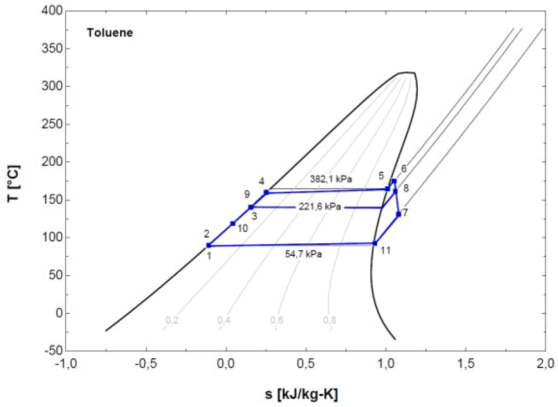

Fig. 3. T-s diagram for the regenerative recuperated superheated ORC.

and safety concerns must also be considered. Although a significant number of working fluids have been considered in the literature, only a very small fraction of them meets the criteria of industrial applications. From the literature review [22,23,29,35–37], toluene has been selected as a working fluid in order to meet with SPTCs outlet temperature and ORC condensing temperature, typical values between 180 and 260 °C, and 80–110 °C, respectively. Some of the thermodynamic properties of toluene are listed in Table 2.

Table 2
Toluene thermodynamic properties [29,38].

Fluid Parameters	Properties
Molecular formula	C_7H_8
Molecular weight	92.14 g/mol
Melting point	−95 °C
Boiling point	110.6 °C
Critical temperature	318.6 °C
Critical pressure	4.1 kPa
Vapor pressure	2.8 kPa

Heat source

The heat input to the ORC is provided by a solar field formed by SPTCs (PTMx-24 from the company Soltigua [39]) with a total collecting area of 617.4 m^2, consisting of five rows with two collectors per row. Solar irradiation is selected to be constant in order the emphasis the comparison analysis and the parametric study of the CCHP system; however, further investigations could cover a dynamic simulation considering solar irradiation variation along the day and along the year. The design parameters of the solar system and the solar collector's specifications are described in Table 3.

For an absorber pipe with a glass envelope, as depicted in Fig. 4, the equations presented in [40] are considered for the energy modeling of the SPTC.

The energy balance in a section of the absorber pipe depends mainly on: *i)* Radiation losses from the glass envelope to the open sky ($\dot{q}'_{57rad}$); *ii)* Convection losses from the glass envelope to the environment ($\dot{q}'_{56conv}$); *iii)* Radiation losses from the selective coating of the metal tube to the glass envelope ($\dot{q}'_{34rad}$); *iv)* Conduction losses through metal pipe supports ($\dot{q}'_{cond,bracket}$).

The working fluid selected in the solar collector receiver is Therminol-66, see Table 4. It is a commercial oil suitable for the temperature range for this application, with low relative pressure and non-sensitive to the increase in the temperature.

Absorption heat pump

Regarding the modeling of the absorption heat-pump, the literature review contains several studies with experimental data validation for H_2O/LiBr absorption heat pumps [42–45]. In the present study, a model with 18 states of a water-cooled single-effect absorption heat pump is proposed. Each state is defined by its temperature, pressure, enthalpy, flow rate, H_2O/LiBr concentration, etc.

Besides the mass and energy balance, UA-LMTD method is proposed for the three heat exchange processes with the external streams, that are evaporator, condenser and absorber [46]. This method is a realistic way to specify the size and performance of a heat exchanger in a single parameter providing that UA is relatively constant throughout each heat exchange process.

Table 5 provides the input data used in the proposed model. The chosen values are reasonable and conservative in order to prevent the crystals formation from the H_2O/LiBr solution.

Thermodynamic modeling

The proposed trigeneration system is thermodynamically assessed from both the first and second law viewpoints, based on mass, energy and exergy balances applied to each component of the system under steady-state conditions. The CCHP system can be divided into several subsystems, such as solar system, ORC, and absorption heat pump. The thermodynamic inlet and outlet states of each component are calculated using the Engineering Equation Solver (EES) software based on the given input data and assumptions.

Table 3
Input data for SPTC model [21,22,39,40].

Parameter	Value
Collector aperture width (w_{ap})	2.36 m
Collector length (L_{SPTC})	26.16 m
Absorber pipe diameter	38.0 mm
Glass envelope diameter	62.0 mm
Number of collectors (N_{SPTC})	10
Solar field outlet temperature (T_i)	200 °C
Ambient temperature (T_{amb})	25 °C
Working pressure (P_{sol})	300 kPa
Sun Temperature (T_{sun})	5,770 K
Direct Normal Irradiance (*DNI*)	800 W/m^2
Solar incident angle	0 °
Wind velocity	3 m/s

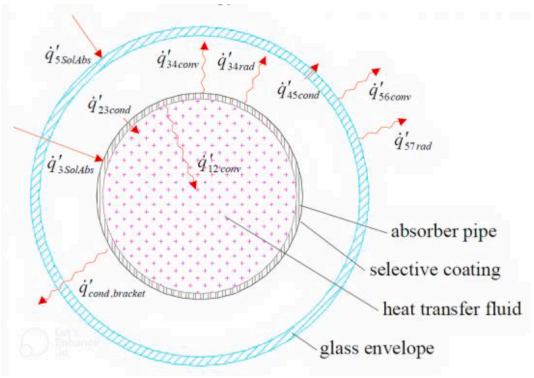

Fig. 4. One-dimensional steady-state energy balance of SPTC [40].

Table 4
Therminol 66 Property Data [41].

Fluid Parameter	Properties
Service temperature	−3 to 345 °C
Density	1020–770 kg/m^3
Specific heat	1.49–2.78 kJ/kg-K
Thermal conductivity	0.118–0.089 W/m-K
Dynamic viscosity	2.92 @110 °C / 0.5 @270 °C mPa-s
Vapor pressure	0.2 @ 280 °C atm

Table 5
Input data for Absorption Heat Pump model [43,46].

Parameter	Value
Maximum solution concentration (X_4)	62 %
Condensation temperature ($T_{11''}$; $T_{13''}$)	25 °C
Condensation mass flow rate ($\dot{m}_c$)	12 kg/s
Evaporation temperature ($T_{16''}$)	7 °C
Evaporation mass flow rate ($\dot{m}_e$)	10 kg/s
Solution heat exchanger efficiency ($\eta_{sol.he}$)	65%
UA evaporator	35 kW/K
UA condenser	45 kW/K
UA absorber	25 kW/K

Energy and exergy analysis relations

The mass and energy balances for each component can be formulated as follows [47]:

$$\sum_{in}\dot{m}_{in}-\sum_{out}\dot{m}_{out}=0 \tag{1}$$

$$\sum_{in}h_{in}\dot{m}_{in}-\sum_{out}h_{out}\dot{m}_{out}+\dot{W}+\dot{Q}=0 \tag{2}$$

The exergy analysis is used to determine the maximum work extractable from a system that interacts in equilibrium with the environment (i.e., dead state). The general exergy balance of a control volume can be written as follows:

$$\sum_{j}\left(1-\frac{T_0}{T_j}\right)\dot{Q}_j-\dot{W}+\sum_{in}\dot{m}_{in}ex_{in}-\sum_{out}\dot{m}_{out}ex_{out}-\dot{E}x_d=0 \tag{3}$$

where $\dot{E}x_d$ and ex are the exergy destruction rate and exergy per unit mass flow rate, respectively. $\dot{Q}_j$ is the heat transfer rate through the boundary at temperature T_j at state j, and $\dot{W}$ is the work rate. The

subscript 0 is the value of the property at dead state conditions.

In the absence of electricity, magnetism, surface tension and nuclear reaction, the total exergy of a system can be divided into four components: physical exergy, kinetic exergy, potential exergy, and chemical exergy [48]. In the present study, the kinetic and potential effects are negligible, so only the physical and chemical components of the exergy are considered. For those subsystems where there is no change in the composition of the fluid, such as the solar system and the ORC, the chemical exergy does not need to be calculated because its value does not change.

The physical exergy per mass flow rate, $\dot{E}x^{ph}$, at a given state is defined as follows [49]:

$$\dot{E}x^{ph} = \dot{m}[(h - h_0) - T_0(s - s_0)] \tag{4}$$

For the mixture or solution of the absorption heat pump, the chemical exergy per mas flow rate, $\dot{E}x^{ch}$, at a given state is calculated by means of [32,50]:

$$\dot{E}x^{ch} = \dot{m}\left[\sum_i X_i\left(\mu_{i,0} - \mu^*_{i,0}\right)\right] \tag{5}$$

where $\mu_{i,0}$ (kJ/kg) is the chemical potential of "i" at the dead state pressure and temperature, and the composition of a given state; $\mu^*_{i,0}$ (kJ/kg) is the chemical potential of "i" at dead state conditions when the system reaches chemical equilibrium with the environment; X_i is the mass fraction of component "i".

$$\dot{E}x = \dot{E}x^{ph} + \dot{E}x^{ch} \tag{6}$$

Exergy is a function of state that relates the first and the second law of thermodynamics through a reference state, that normally coincides with the surrounding environment. A system is said to be in thermodynamic equilibrium with the surroundings when it is in thermal, mechanical, and chemical equilibrium [51]. However, the definition of the reference state is not trivial and can impacts on the analysis results. Most of the cited authors assumed that the dead state pressure should equal atmospheric pressure. Some other authors propose a reference environment defined as the variable outdoor environment surrounding the application of the thermal system [52–54] following a dynamic approach, and, thus, representing a more complex analysis.

In this study, the CCHP system is divided in the following subsystems: the solar system, the ORC, and the absorption heat pump. All the working fluids for each subsystem are confined as closed-loop, thus, none of them are directly in contact with the environment. They are unable to maintain a balance with the environment surrounding the system, either in terms of pressure or composition. For this case, Gaggioli [55] proposes as dead state the state reached when the system was shut down, once the system reaches the thermal equilibrium with the environment.

Ambient temperature ($T_0 = 25\ ^\circ$C) is selected as dead state condition for all the subsystems. However, a different dead state condition for pressure is selected here for each subsystem. For the solar field, despite the thermal oil properties are not influenced by pressure, the dead state pressure can be taken as an intermediate value between the working pressure of the Therminol-66 and the ambient pressure; here, $P_{0,sol} =$ 150 kPa. For the ORC subsystem, the appropriate dead state pressure ($P_{0,ORC}$) would be the working fluid saturation pressure at T_0 [48]. For the absorption heat pump subsystem, according to Blanco-Marigorta and Marcos [32] and Viswanathan et al. [56], the dead state pressure can be taken as the pressure of state 1 ($P_{0,hp} = P_1$). The composition of the dead state is calculated when the chemical equilibrium is reached, then $X_{0,LiBr}(T_{0,hp}, P_{0,hp})$.

CCHP performance indexes

This section presents the formulation of the performance assessment of the CCHP system. The energy and exergy efficiency ratios of the net electricity generation by the ORC are presented in Eq. (7)–(8). According to Eq. (12), the Petela model [57] is used for the calculation of the exergy flow of the solar irradiation, $\dot{E}x_{in}$.

$$\eta_{en,el} = \frac{\dot{W}_{turb} - \dot{W}_{ORC,pump}}{\dot{Q}_{sol}} \tag{7}$$

$$\eta_{ex,el} = \frac{\dot{W}_{turb} - \dot{W}_{ORC,pump}}{\dot{E}x_{in}} \tag{8}$$

where:

$$\dot{W}_{turb} = \dot{m}_{ORC}h_6 - \dot{m}_{ORC,A}h_7 - \dot{m}_{ORC,B}h_8 \tag{9}$$

$$\dot{W}_{ORC,pump} = \dot{m}_{ORC,A}(h_2 - h_1) + \dot{m}_{ORC}(h_3 - h_9) \tag{10}$$

$$\dot{Q}_{sol} = DNI\ w_{ap}\ L_{SPTC}\ N_{SPTC} \tag{11}$$

$$\dot{E}x_{in} = \dot{Q}_{sol}\left[1 - \frac{4}{3}\frac{T_0}{T_{sun}} + \frac{1}{3}\left(\frac{T_0}{T_{sun}}\right)^4\right] \tag{12}$$

The energy and exergy efficiency ratios of the trigeneration system are formulated as:

$$\eta_{en,tri} = \left(\frac{\dot{W}_{turb} - \dot{W}_{ORC,pump} - \dot{W}_{S,pump} + \dot{Q}_{cool} + \dot{Q}_{heat}}{\dot{Q}_{sol}}\right) \tag{13}$$

$$\eta_{ex,tri} = \left(\frac{\dot{W}_{turb} - \dot{W}_{ORC,pump} - \dot{W}_{S,pump} + \dot{E}_{P,cool} + \dot{E}_{P,heat}}{\dot{E}x_{in}}\right) \tag{14}$$

where

$$\dot{Q}_{cool} = \dot{m}_e(h_{15''} - h_{16''}) \tag{15}$$

$$\dot{Q}_{heat} = \dot{m}_c[(h_{12''} - h_{11''}) + (h_{14''} - h_{13''})] \tag{16}$$

$$\dot{W}_{S,pump} = \dot{m}_{S,hp}(h_{2''} - h_{1''}) \tag{17}$$

$$\dot{E}_{P,cool} = \dot{E}x_{16''} - \dot{E}x_{15''} \tag{18}$$

$$\dot{E}_{P,heat} = \left(\dot{E}x_{12''} - \dot{E}x_{11''}\right) + \left(\dot{E}x_{14''} - \dot{E}x_{13''}\right) \tag{19}$$

The overall efficiency of the solar collector considers all types of losses described previously (i.e., optical, geometric and thermal), and it can be defined as the ratio between the useful thermal energy supplied to the solar thermal oil, and the available solar energy based on the Direct Normal Irradiance (DNI).

$$\eta_{SPTC} = \frac{\dot{q}'_u}{\dot{q}'_{sol}} = \frac{\dot{q}'_u}{DNI\ w_{ap}} \tag{20}$$

where $\dot{q}'_u$ is defined as

$$\dot{q}'_u = \frac{\dot{m}_{SPTC}Cp_{oil}(T_{sol.out} - T_{sol.in})}{L_{SPTC}} \tag{21}$$

The coefficient of performance (COP) of the heat pump for cooling and heating mode is defined as

$$COP_c = \frac{\dot{Q}_{cool}}{\dot{Q}_d + \dot{W}_{S,pump}} \tag{22}$$

$$COP_h = \frac{\dot{Q}_{heat}}{\dot{Q}_d + \dot{W}_{S,pump}} \quad (23)$$

Where

$$\dot{Q}_d = \dot{m}_{ORC}(h_{11} - h_1) \quad (24)$$

For a better understanding of the exergy performance of the specific components and subsystems z of the trigeneration system, additional parameters are calculated through specific exergy balances following a fuel-product formulation [33].

$$\dot{E}_{F,z} - \dot{E}_{P,z} = \dot{E}_{D,z} - \dot{E}_{L,z} \quad (25)$$

$$\eta_{ex,z} = \frac{\dot{E}_{P,z}}{\dot{E}_{F,z}} \quad (26)$$

where $\dot{E}_{F,z}$ corresponds to the fuel exergy, $\dot{E}_{P,z}$ is the product exergy, $\dot{E}_{D,z}$ is the destroyed exergy, and $\dot{E}_{L,z}$ is the exergy loss.

Assuming that the waste heat produced in the condenser and absorber of the absorption heat pump can also be usable for low temperature heating processes, the exergy loss of the CCHP system can be considered zero.

Exergy balance in the Solar field:

$$\dot{E}_{F,sol} = \dot{E}x_{in} \quad (27)$$

$$\dot{E}_{P,sol} = \dot{E}x_{1'} - \dot{E}x_{4'} \quad (28)$$

$$\eta_{ex,sol} = \frac{\dot{E}_{P,sol}}{\dot{E}_{F,sol}} \quad (29)$$

Exergy balance in the ORC:

$$\dot{E}_{F,ORC} = \dot{E}x_{1'} - \dot{E}x_{4'} \quad (30)$$

$$\dot{E}_{P,ORC} = \dot{W}_{turb} - \dot{W}_{ORC,pump} - \left(\dot{E}x_{11} - \dot{E}x_1\right) \quad (31)$$

$$\eta_{ex,ORC} = \frac{\dot{E}_{P,ORC}}{\dot{E}_{F,ORC}} \quad (32)$$

Exergy balance in the Absorption heat pump:

$$\dot{E}_{F,hp} = \left(\dot{E}x_{11} - \dot{E}x_1\right) + \dot{W}_{S,pump} \quad (33)$$

$$\dot{E}_{P,hp} = \dot{E}_{P,cool} + \dot{E}_{P,heat} \quad (34)$$

$$\eta_{ex,hp} = \frac{\dot{E}_{P,hp}}{\dot{E}_{F,hp}} \quad (35)$$

The fuel-product formulation cannot be directly applied to dissipative elements like the expansion valves of the absorption heat pump, therefore, the approach followed in this paper is to consider the valve as elements that serve the evaporator and absorber [58].

The relation between the destroyed exergy of a component k with the total fuel exergy of the system can be defined as the exergy destruction ratio ($Y_{D,k}$), and it is formulated as:

$$Y_{D,k} = \frac{\dot{E}_{D,k}}{\dot{E}x_{in}} \quad (36)$$

The irreversibility ratio of a component k, which relates the destroyed exergy of a component and the total destroyed exergy of the system, is defined as

$$Y^*_{D,k} = \frac{\dot{E}_{D,k}}{\dot{E}_{D,Tot}} \quad (37)$$

Validation of the system

There is lack in experimental data of a similar trigeneration system in literature; hence, with the aim to validate the accuracy of the proposed modeling, three different validation procedures are described for each subsystem.

The validation of the solar collectors model is conducted by comparing the heat losses of the SPTC with test results reported by Dudley et al. [59] at Sandia National Laboratory. The validation results are based on the design data for the black chrome receiver material case for a vacuum space between the absorber pipe and the glass envelope, and are shown in Table 6 and Fig. 5-a. Moreover, the model is compared to the numerical results obtained from Ref. [24,28]. In the present study, the solar driven CCHP system is examined for an absorber fluid temperature ranging 150–230 °C above ambient temperature. Therefore, the proposed SPTC model is in good agreement with the experimental results and the simulation outcomes of the mentioned literature. The deviation in the calculations can be mainly attributed to differences in geometry and size of the SPTC proposed in the study, the thermal correlations, and the approximations used to calculate the heat loss coefficients (i.e., boundary conditions, mass flow rates, etc).

Regarding the ORC, the developed model is compared with literature results from Branchini et al. [7] because this is the only study where an ORC layout with toluene as organic working fluid is examined in detailed. The examined parameter for the validation is $\eta_{en,el}$ versus the evaporation pressure, normalized with respect to the critical pressure (P_{eva}/P_{cr}) of the working fluid. To conduct an appropriate comparison, some changes are made to the developed model; for instance, the condensation temperature was set equal to 33 °C. In this study, the CCHP system is examined for a solar field outlet temperature ranging 180–260 °C, equals to a value of P_{eva}/P_{cr} in the range 0.07–0.3. The validation results reported in Table 7 and Fig. 5-b show that the ORC model is in good agreement with the results of the mentioned literature.

Finally, the absorption heat pump model is validated with experimental data presented by Bakhtiari et al. [43] for a laboratory single-stage H_2O/LiBr absorption heat pump. This literature study is selected because the COP for cooling operation is analysed for different generator inlet temperature as it is the case for the present investigation. Some modifications have been made in the input data of the model in order to perform an appropriate comparison with the literature results, such as the mass flow rates for the external loops. The comparison results presented in Table 8 show small deviation up to 2.7% for the COP. The deviation is higher on the desorber and evaporator heat loads; nevertheless, the model agrees well with the experimental results. The deviation in the calculations is attributed to the approximation used for the overall heat transfer coefficients for each heat exchangers.

Results and discussion

The methodology followed to evaluate the proposed solar-trigeneration system from the energy and exergy viewpoints is organized as follow. First, a detailed exergy analysis is conducted to assess the exergy performance and to identify and quantify the sources of the exergy destruction in the system considered. Then, a parametric

Table 6
Validation of the SPTC model based on heat loss versus average temperature above the ambient of the fluid inside the absorber pipe.

	Temperature [°C]	149.1	196.7	245.8	293.3
Heat loss [W/m^2]	This study	25.2	31.7	41.9	56.2
	Ref [59]	19.3	30.6	45.4	62.9
	Deviation	30.5%	3.7%	7.7%	10.6%
	Ref [24]	19.3	34.2	53.0	75.5
	Deviation	30.5%	7.2%	20.9%	25.5%
	Ref [28]	19.7	34.4	52.5	74.5
	Deviation	27.8%	7.8%	20.2%	24.5%

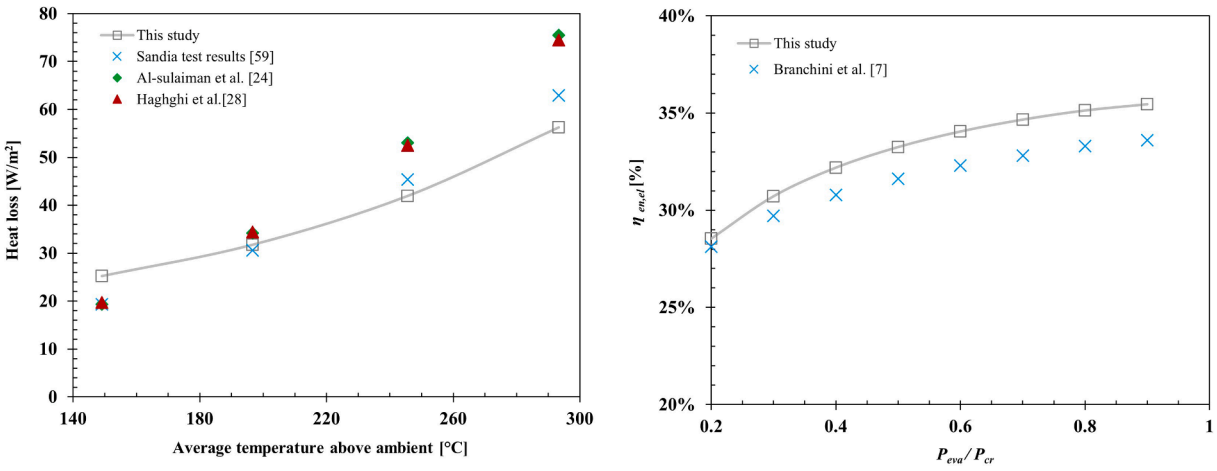

Fig. 5. Validation of the SPTC model (a) and ORC model (b).

Table 7
Validation of the ORC model based on energy efficiency versus the evaporation pressure, normalized with respect to the critical pressure.

	P_{eva}/P_{cr}	0.2	0.3	0.4	0.5	0.6	0.7	0.8	0.9
$\eta_{en,el}$ [%]	This study	28.54	30.72	32.19	33.25	34.05	34.66	35.13	35.45
	Ref [7]	28.12	29.71	30.79	31.62	32.29	32.81	33.29	33.60
	Deviation	1.5%	3.4%	4.5%	5.2%	5.5%	5.6%	5.5%	5.5%

Table 8
Validation of the heat pump model based on COP and heat loads versus generator inlet temperature.

Temperature [°C]			COP			$\dot{Q}_d$ [kW]			$\dot{Q}_{cool}$ [kW]		
T_{11}	$T_{16''}$	$T_{11''}$	This study	Ref [43]	Deviation	This study	Ref [43]	Deviation	This study	Ref [43]	Deviation
79.9	26.8	14.9	0.75	0.76	1.3%	11.0	13.5	18.5%	8.2	10.2	19.6%
89.9	27.1	15.2	0.76	0.76	0.0%	14.7	15.9	7.5%	11.2	12.1	7.4%
100.1	27.2	15.1	0.76	0.74	2.7%	18.4	20.4	9.8%	14.0	15.2	7.9%
109.7	26.8	14.9	0.75	0.73	2.7%	22.2	22.8	2.6%	16.8	16.5	1.8%

approach is conducted with the aim to evaluate the effects of different system parameters on the energy and exergy efficiency for the power generation and for the overall CCHP system. Finally, the system is optimized based on the same operating parameters under different optimization criteria using single and multi-objects approaches.

Energy and exergy analysis

A detailed exergy analysis is presented and discussed in this section. The objective is to identify and quantify the sources of the exergy destruction in the overall CCHP system through an exergetic assessment of all the components of the trigeneration system. The thermodynamic properties of the streams for the design conditions are shown in Table 9. On the other hand, Table 10 provides important information about the sources of irreversibility and key exergy parameters, such as the exergy rate of the fuel and the product, the exergy efficiency, the exergy destruction rate, the exergy destruction ratio, and the irreversibility ratio. The results indicate that the main source of exergy destruction is the solar collectors, 335.6 kW (85%). The absorption heat pump destroys 38 kW (10%), while the ORC 18.7 kW (5%). It is important to note the low contribution of the ORC in the total exergy destruction compared to similar CCHP systems found in the literature [24,26,28]. In those systems, the ORC accounted for 28%, 25%, and 32% of the total exergy destruction, respectively. This finding demonstrates the soundness of choosing the regenerative recuperated superheated cycle.

Fig. 6 shows the fuel and product exergy rate of the overall trigeneration system, and the destroyed exergy rate of each subsystem. The exergy efficiency found for the solar subsystem is 27.0%, for the ORC is 84.9%, and for the absorption heat pump is 31.4%. The main reason of the large exergy destruction in the SPTCs (335 kW) is the high temperature difference between the collector and the environment, what provokes important heat losses in the receiver, thus, special attention needs to be paid on the selection and design of an efficient component.

The overall exergy destruction rates and their percentage are represented in Fig. 7. Specifically for the absorption heat pump, the percentage share of the exergy destruction by each component is as follows: desorber 31%, absorber 30%, evaporator 18%, condenser 13%, and solution HX 8%. There are relevant works in the literature focused on the exergy analysis of single H_2O/LiBr absorption systems at component level. However, few of them consider the calculation of the chemical exergy of the streams. Fig. 8 shows a comparison of the exergy destroyed in the different components with the results obtained by other authors [32,60–62]. No major differences with the other authors are identified. The most significant deviations are found in the condenser and absorber, where the values obtained are −6% and + 5%, respectively, with respect to the average results of the other authors.

Parametric analysis

Effect of the outlet temperature of the solar field

The energy source provided by the solar field is what determines the ORC's optimal evaporation temperature. The purpose of this study is to show the effect of varying the output temperature of the solar field in the range of 180 to 260 °C on the efficiency of the ORC and on the overall CCHP system. Table 11 and Fig. 9 represents the performance of the system as well as the power and thermal energy generation.

Table 9
Thermodynamic properties of the streams.

Subsystem	State no.	Fluid	$\dot{m}$[kg/s]	T[°C]	P[kPa]	h[kJ/kg]	s[kJ/kgK]	$\dot{E}x^{ph}$[kW]	$\dot{E}x^{ch}$[kW]	$\dot{E}x$[kW]
Solar	**1′**	Therminol-66	5.34	200	300	378.5	1.031	394.0		368.8
	2′	Therminol-66	5.34	198.6	300	375.4	1.025	388.1		363.0
	3′	Therminol-66	5.34	172	300	318.7	0.900	282.9		260.2
	4′	Therminol-66	5.34	168.7	300	311.5	0.884	269.7		243.4
ORC	**1**	Toluene	0.815	90	54.7	−40.5	−0.108	9.3		9.4
	2	Toluene	0.815	90.1	221.6	−40.2	−0.108	9.5		9.5
	3	Toluene	0.913	140.6	382.1	62.1	0.155	32.5		24.9
	4	Toluene	0.913	160	382.1	103.9	0.253	43.8		41.6
	5	Toluene	0.913	165	382.1	435.9	1.011	140.8		133.8
	6	Toluene	0.913	175	382.1	454.0	1.052	146.2		139.0
	7	Toluene	0.815	131	54.7	394.0	1.079	75.2		76.2
	8	Toluene	0.098	161.7	221.6	437.0	1.059	13.8		5.43
	9	Toluene	0.913	140.5	221.6	61.7	0.154	32.3		24.7
	10	Toluene	0.815	118.8	221.6	16.6	0.042	19.2		19.4
	11	Toluene	0.815	92.7	54.7	337.3	0.931	64.7		65.6
Absorption heat pump	**1″**	water-LiBr	1.165	34.6	0.75	89.7	0.211	0.36	5.53	5.89
	2″	water-LiBr	1.165	34.6	5.07	89.7	0.211	0.36	5.53	5.89
	3″	water-LiBr	1.165	60.0	5.07	141.0	0.369	4.48	5.53	10.01
	4″	water-LiBr	1.068	80.5	5.07	202.9	0.451	9.31	18.35	27.66
	5″	water-LiBr	1.068	50.7	5.07	147.1	0.285	2.10	18.35	20.45
	6″	water-LiBr	1.068	45.2	0.75	147.1	0.253	1.32	18.35	19.67
	7″	water	0.097	69.3	5.07	2,629.4	8.599	26.13		26.13
	8″	water	0.097	33.1	5.07	138.8	0.479	19.22		19.22
	9″	water	0.097	2.8	0.75	138.8	0.503	18.54		18.54
	10″	water	0.097	2.8	0.75	2,505.7	9.08	0.15		0.15
	11″	water	12	25.0		104.5	0.367	0		0
	12″	water	12	30.9		129.4	0.450	3.07		3.07
	13″	water	12	25.0		104.8	0.367	0		0
	14″	water	12	29.8		124.9	0.434	2.08		2.08
	15″	water	10	12.5		52.4	0.187	10.97		10.97
	16″	water	10	7.0		29.4	0.106	23.23		23.23

Table 10
Results of the exergy analysis of all the components of the CCHP system.

Subsystem	Component	$\dot{W}o\dot{Q}$ [kW]	$\dot{E}_F$[kW]	$\dot{E}_P$[kW]	$\dot{E}_D$[kW]	η_{ex}[%]	Y_D	Y^*_D
Solar	**SPTCs**	358.1	459.9	124.3	335.6	27.0	72.98	85.53
ORC	**Economizer**	38.2	13.2	11.3	1.9	85.6	0.41	0.48
	Evaporator	303.3	105.2	97.0	8.2	92.2	1.78	2.09
	Superheater	16.6	5.8	5.4	0.4	92.8	0.09	0.11
	Turbine	50.6	57.2	50.6	6.6	88.4	1.44	1.68
	Recuperator	46.3	10.4	9.7	0.7	93.2	0.15	0.18
	Regenerator	56.4	33.0	32.2	0.8	97.6	0.17	0.20
	ORC Pump 1	0.24	0.24	0.18	0.06	75.4	0.01	0.01
	ORC Pump 2	0.28	0.28	0.22	0.06	78.4	0.01	0.01
Absorption heat pump	**Desorber**	308.0	55.4	43.7	11.7	78.9	2.53	2.97
	Evaporator	230.0	19.1	12.3	6.8	64.3	1.47	1.73
	Absorber	295.0	14.7	3.1	11.6	20.8	2.53	2.97
	Condenser	242.0	6.9	2.1	4.8	30.2	1.05	1.23
	Solution HX	59.7	7.2	4.1	3.1	57.2	0.67	0.78
	Total	–	–	–	392.4	–	–	100

As it can be observed, as the solar field outlet temperature increases, both the electrical and trigeneration energy and exergy efficiencies increase, while the exergy destruction rate decreases. This is because a higher heat source temperature results in a higher working liquid evaporator pressure in the ORC, resulting in a higher heat recovery efficiency in the evaporator. As long as the exergy loss is lower than the exergy destruction, the exergy efficiency exhibits an inverse relationship with the exergy destruction rate. Thus, an increase in the solar field outlet temperature results in a decrement in the amount of exergy destroyed.

When the heat source's inlet temperature rises from 180 °C to 260 °C, the rate of increase for the electrical energy and exergy efficiencies is 92%, the power generated in the turbine is double, and the rate of decrease for the destroyed exergy is 8%.

Effect of the condensation temperature of the ORC

The desorber of the absorption heat pump, coupled in cascade to the ORC, requires a specific amount of heat input within a defined

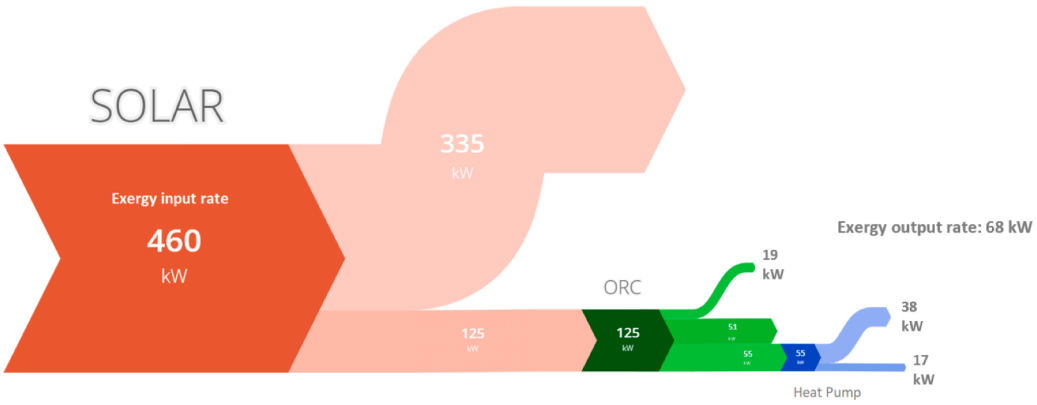

Fig. 6. Grassmann's diagram of the CCHP system.

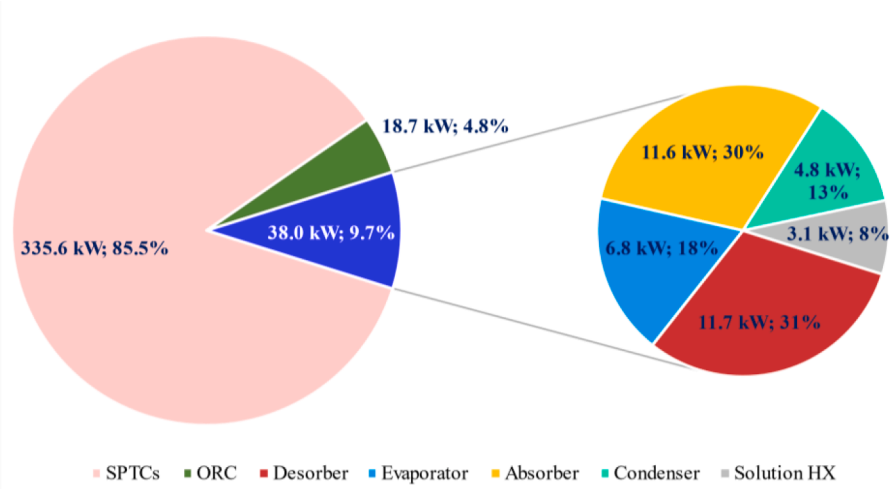

Fig. 7. Overall exergy destruction rates and percentages.

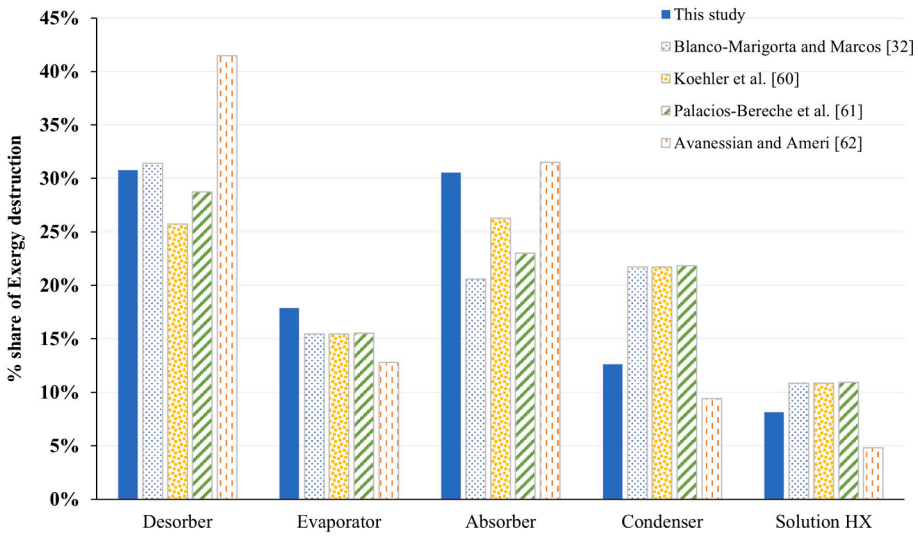

Fig. 8. Percentage share of the exergy destruction in the absorption heat pump.

temperature range to operate effectively. The inlet temperature is governed by the ORC condensation temperature, making it crucial to determine the optimal operating temperature based on preferred cooling and heating generation, without compromising the ORC performance. The impact of the ORC condensation temperature is examined in the range 80–105 °C, and systems energy and exergy performances, as well as electrical and thermal generation are presented in Table 12 and Fig. 10.

The ORC condensation temperature proves to be an effective parameter for regulating the absorption heat pump's capacity to

Table 11
Results of the parametric simulation with the outlet temperature of the solar field (T_i).

T_i [°C]	$\eta_{en,el}$[%]	$\eta_{ex,el}$[%]	$\eta_{en,tri}$[%]	$\eta_{ex,tri}$[%]	$\dot{W}_{turb}$[kW]	$\dot{Q}_{cool}$[kW]	$\dot{Q}_{heat}$[kW]	COP_c	$\dot{E}_{D,Tot}$[kW]	$\dot{E}_{D,Sol}$[kW]	$\dot{E}_{D,ORC}$[kW]	$\dot{E}_{D,hp}$[kW]	$\eta_{ex,sol}$[%]	$\eta_{ex,ORC}$[%]	$\eta_{ex,hp}$[%]
180	7.90	8.49	168.2	12.40	39.4	235.6	556.2	0.735	402.9	344.8	18.3	39.7	25.02	84.06	31.21
190	9.06	9.73	166.9	13.58	45.2	232.8	547.0	0.741	397.4	339.8	18.8	38.8	26.11	84.34	31.33
200	10.14	10.89	165.6	14.67	50.6	230.0	538.0	0.747	392.4	335.6	18.8	38.0	27.02	84.89	31.42
220	12.07	12.97	162.9	16.63	60.5	224.2	520.8	0.756	383.4	325.8	21.1	36.5	29.16	84.26	31.56
240	13.75	14.76	160.2	18.31	69.1	218.4	504.7	0.763	375.7	318.3	22.2	35.2	30.79	84.32	31.65
260	15.18	16.30	157.4	19.74	76.7	212.8	489.5	0.769	369.1	310.8	24.3	34.0	32.41	83.71	31.71

produce cooling and heating. The results demonstrate that as the ORC condensation temperature increases, both the electrical and trigeneration energy and exergy efficiencies decrease. This decrease is attributed to the fact that with decreasing condensing pressure (and thus temperature), the capacity to extract work in the turbine of the ORC increase while the heat input to the desorber of the heap pump decreases.

When the ORC condensation temperature rises from 80 °C to 105 °C, the rate of decrease in the electrical energy and exergy efficiencies, as well as power generated in the turbine, amounts to 30%. On the other hand, the rate of increase in the destroyed exergy is 4%. In contrast, the overall CCHP energy efficiency increases as the ORC condensation temperature rises; this is due to the increased heat input supplied to the desorber, resulting in higher production levels in the evaporator, absorber and condenser.

Effect of the heat pump evaporation temperature

Variations in the external temperatures have an impact on the absorption heat pump's performance. The effect of the evaporation temperature of the absorption heat pump is evaluated in this section. The evaporation temperature ($T_{16''}$) is examined from 5 to 15 °C, and the variation of the COP, the cooling capacity and the exergy indicators are presented in Table 13 and Fig. 11.

The evaporation temperature of the heat pump is a crucial design parameter of the trigeneration system. The selection of this parameter depends on the specific cooling application; for instance, air conditioning applications in commercial buildings based on fan-coils units requires chilled water at 7 °C, while radiant systems can operate at 12 °C. The results indicate that as the evaporation temperature increases, both the cooling and heating production, as well as the COP_c and COP_h increase. However, both the trigeneration and heat pump exergy efficiencies decrease. The rate of decrease for the heat pump exergy efficiency within the analysed range amounts to 37%.

Optimization of the system

The optimization procedure analysed in this section is based on single and multi-objective approaches. The operating parameters are simultaneously varied in their specific range, see Table 14. From the several optimization methods are available in the EES software, the conjugate directions method is used.

The traditional weighted-sum method is used for multi-objective optimization for the present study. This method combines all the single-objective functions into one scalar by adding the corresponding objectives with appropriate weights [63,64]. For the proposed CCHP system, different multi-objective functions (MOF) with some appropriate weights are considered based on different objectives selected.

$$\begin{aligned} &MAX(MOF_1 = w_1\dot{W}_{turb} + w_2\dot{Q}_{cool}) \\ &0 \le w_1, w_2 \le 1 \\ &w_1 + w_2 = 1 \end{aligned} \tag{38}$$

$$\begin{aligned} &MAX(MOF_2 = w_1\eta_{ex,el} + w_2\eta_{en,tri} + w_3\eta_{ex,tri}) \\ &0 \le w_1, w_2, w_3 \le 1 \\ &w_1 = 1/3; w_2 = 1/3 \\ &w_1 + w_2 + w_3 = 1 \end{aligned} \tag{39}$$

The results presented in Table 15 outline all the optimum solutions, as well as the default case, for the analysed trigeneration system following different optimization criteria based on single and multi-objective methods. These results provide a range of optimal designs, each with their own set of benefits and drawbacks. This enables the designer to choose those design conditions that best suit the project requirements. When considering the overall exergy efficiency as the sole optimization goal, the emphasis is placed on electricity production. In this scenario, the power generated by the ORC is 62% higher than the default case. However, both the cooling and heating production decrease by approximately 13%. When both power generation and

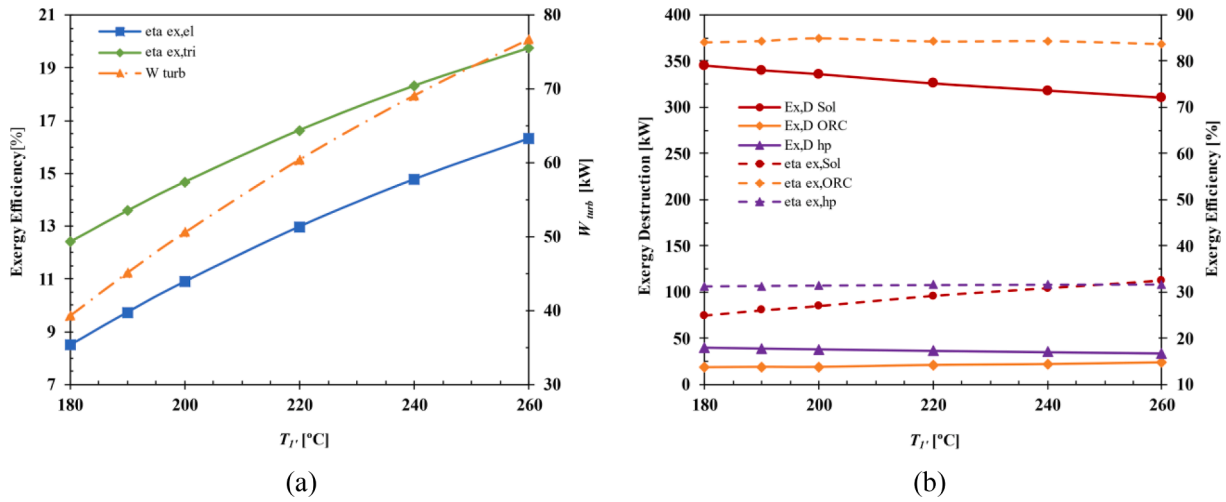

Fig. 9. Effect of the outlet temperature of the solar field on the system performance (a) and on the exergy destruction rate and exergy efficiency (b).

Table 12
Results of the parametric simulation with the condensation temperature of the ORC (T_1).

T_1 [°C]	$\eta_{en,el}$ [%]	$\eta_{ex,el}$ [%]	$\eta_{en,tri}$ [%]	$\eta_{ex,tri}$ [%]	$\dot{W}_{turb}$ [kW]	$\dot{Q}_{cool}$ [kW]	$\dot{Q}_{heat}$ [kW]	COP_c	$\dot{E}_{D,Tot}$ [kW]	$\dot{E}_{D,ORC}$ [kW]	$\dot{E}_{D,hp}$ [kW]	$\eta_{ex,ORC}$ [%]	$\eta_{ex,hp}$ [%]
80	11.46	12.30	164.3	16.02	57.1	226.7	528.2	0.752	386.2	20.5	30.1	83.55	36.19
85	10.80	11.60	165.0	15.35	53.9	228.4	533.1	0.749	389.3	19.6	34.1	84.24	33.61
90	10.14	10.89	165.6	14.67	50.6	230.0	538.0	0.747	392.4	18.8	38.0	84.89	31.42
95	9.47	10.17	166.3	13.99	47.3	231.5	542.8	0.744	395.5	18.0	41.9	85.51	29.54
100	8.80	9.45	166.9	13.30	44.0	233.1	547.7	0.741	398.7	17.3	45.8	86.09	27.91
105	8.12	8.72	167.5	12.61	40.6	234.5	552.5	0.738	401.9	16.6	49.7	86.64	26.47

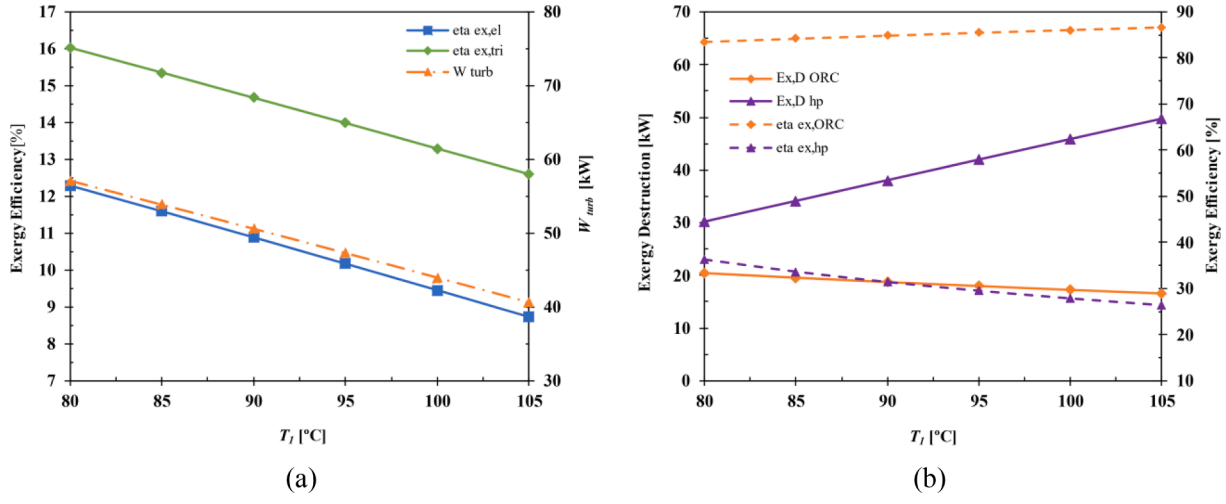

Fig. 10. Effect of the ORC condensation temperature on the system performance (a) and on the exergy destruction rate and exergy efficiency (b).

Table 13
Results of the parametric simulation with heat pump evaporation temperature ($T_{16''}$).

$T_{16''}$ [°C]	$\eta_{en,tri}$ [%]	$\eta_{ex,tri}$ [%]	$\dot{Q}_{cool}$ [kW]	$\dot{Q}_{heat}$ [kW]	COP_c	COP_h	$\dot{E}_{D,Tot}$ [kW]	$\dot{E}_{D,hp}$ [kW]	$\eta_{ex,hp}$ [%]
5	160.1	14.85	216.4	524.5	0.703	1.703	391.6	37.2	32.89
7	165.6	14.67	230.0	538.0	0.747	1.747	392.4	38.0	31.42
10	170.4	14.25	241.8	549.8	0.785	1.785	394.4	40.0	27.87
12	172.7	13.92	247.5	555.5	0.804	1.804	395.9	41.5	25.15
15	175.7	13.39	254.9	562.9	0.828	1.828	398.3	43.9	20.80

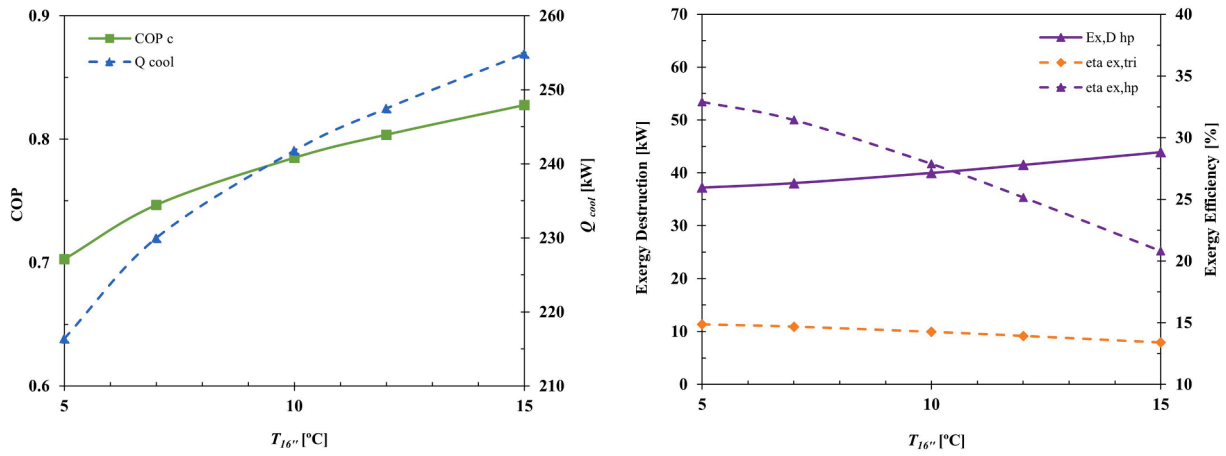

Fig. 11. Effect of the evaporation temperature on the heat pump performance (a) and on the exergy destruction rate and exergy efficiency (b).

Table 14
Optimization variables.

Parameter	Default value	Examined range
Solar field outlet temperature (T_i)	200 °C	[180–260] °C
ORC Condensation temperature (T_1)	90 °C	[80–105] °C
Heat pump evaporation temperature ($T_{16''}$)	7 °C	[5–15] °C

cooling production are used as optimization targets, the performance indicators are higher than those of the default case, but lower that for the exergy efficiency optimum.

Conclusions

A complete thermodynamic analysis of a solar driven ORC-absorption based CCHP system is conducted following a novel exergy approach not used so far for trigeneration applications. Key questions related to the exergy assessment of the proposed system are identified and addressed. The proposed CCHP system can produce electricity, heating and cooling simultaneously from a clean energy source, such as solar energy, which makes this technology a highly competitive solution to be used in buildings and industries applications as opposed to conventional fossil fuel energy systems. The following findings can be concluded from this study:

- Each subsystem is formed by confined working fluids that are not in mechanical equilibrium with the environment. Therefore, the environmental pressure is not selected here as dead state condition. Instead, a different dead state pressure is selected for each subsystem individually.
- In the exergy calculation, chemical exergy must not be neglected in the analysis of the absorption heat pump due to the chemical separation processes involved.
- For the default case, the main source of exergy destruction is the SPTCs, which account for 85% of the total exergy destructed. This is followed by the desorber and the absorber of the absorption heat pump, each contributing 3% to the total exergy destruction. The energy and exergy efficiency ratios found are: 10.1% and 10.9%, respectively for the ORC, and 165.6% and 14.7%, respectively for the trigeneration. The electricity, cooling and heating productions are 50.6 kW, 230.0 kW and 538.0 kW, respectively.
- As the solar field outlet temperature increases, both the energy and exergy efficiency of the CCHP system increase. In the analysed range, the net power produced in the ORC can be doubled.
- The electrical energy and exergy efficiency ratios decrease as the ORC condensation temperature increases. The rate of decrease in the analysed temperature range is about 30%.
- As the evaporation temperature of the absorption heat pump increases, both the cooling and heating production, as well as the COP, increase. However, both the trigeneration and heat pump exergy efficiencies decrease.
- The utilization of different optimization methods yields varied results, providing the designer with the flexibility to tailor the system's operation to specific requirements. Electricity generation significantly influences the exergy efficiency of the overall system. The highest exergy efficiency values can be attained through the utilization of single-objective optimization techniques, with values of 21.1% and 17.5% achieved for the overall system and the ORC, respectively.

The exergy efficiency of the overall trigeneration system is primarily influenced by the low exergy efficiency rates of both the SPTC and the absorption heat pump. Enhancing the utilization of the inlet exergy would lead to higher performance rates. To achieve this, future developments of this work will explore design modifications for certain components and different system layout modifications, aiming to optimize the utilization of the solar source. Additionally, the incorporation of double-stage absorption refrigeration systems, which exhibit higher COP values, will also be considered.

Table 15
Optimization results with various optimization criteria.

Optimization criteria	T_i [°C]	T_1 [°C]	$T_{16''}$ [°C]	$\eta_{en,el}$ [%]	$\eta_{ex,el}$ [%]	$\eta_{en,tri}$ [%]	$\eta_{ex,tri}$ [%]	$\dot{W}_{turb}$ [kW]	$\dot{Q}_{cool}$ [kW]	$\dot{Q}_{heat}$ [kW]	COP_c	$\dot{E}_{D,Tot}$ [kW]
Default case	200	90	7	10.14	10.89	165.6	14.67	50.6	230.0	538.0	0.747	392.4
$\eta_{ex,tri}$	260	80	5	16.27	17.48	152.4	**21.06**	82.1	200.4	471.7	0.738	363.1
$\eta_{en,tri}$	180	104.3	15	5.82	6.25	**182.5**	8.96	29.0	270.8	601.6	0.818	418.6
$\dot{W}_{turb}$, $\dot{Q}_{cool}$	247.3	80	15	15.43	16.57	161.4	18.77	**77.6**	**228.6**	505.6	0.825	373.6
$\eta_{ex,el}$, $\eta_{en,tri}$, $\eta_{ex,tri}$	210.9	80	15	12.49	**13.42**	**170.7**	**15.79**	62.4	243.1	538.5	0.822	387.3

Funding

This work was funded by the Universidad Nacional de Educación a Distancia through the grants to support teaching and research activity (2023-ETSII-UNED-07).

CRediT authorship contribution statement

Jesús García-Domínguez: Conceptualization, Methodology, Software, Formal analysis, Investigation, Resources, Data curation, Writing – original draft, Writing – review & editing, Visualization. **Ana M. Blanco-Marigorta:** Conceptualization, Methodology, Software, Validation, Formal analysis, Resources, Writing – review & editing. **J. Daniel Marcos:** Conceptualization, Methodology, Validation, Formal analysis, Resources, Writing – review & editing, Supervision, Project administration, Funding acquisition.

Declaration of Competing Interest

The authors declare that they have no known competing financial interests or personal relationships that could have appeared to influence the work reported in this paper.

Data availability

Data will be made available on request.

References

[1] Jradi M, Riffat S. Tri-generation systems: energy policies, prime movers, cooling technologies, configurations and operation strategies. Renew Sustain Energy Rev 2014;32:396–415.
[2] Wieland C, Schifflechner C, Dawo F, Astolfi M. The organic Rankine cycle power systems market: recent developments and future perspectives. Appl Therm Eng 2023;224:119980.
[3] Colonna P, Casati E, Trapp C, Mathijssen T, Larjola J, Turunen-Saaresti T, et al. Organic rankine cycle power systems: from the concept to current technology, applications, and an outlook to the future. J Eng Gas Turbines Power 2015;137 (10):100801.
[4] Vélez F, Segovia JJ, Martín MC, Antolín G, Chejnec F, Quijano A. A technical, economical and market review of organic Rankine cycles for the conversion of low-grade heat for power generation. Renew Sustain Energy Rev 2012;16(6):4175–89.
[5] Quoilin S, Van Den Broek M, Declaye S, Dewallef P, Lemort V. Techno-economic survey of Organic Rankine Cycle (ORC) systems. Renew Sustain Energy Rev 2013; 22:168–86.
[6] Lecompte S, Huisseune H, van den Broek M, Vanslambrouck B, De Paepe M. Review of organic Rankine cycle (ORC) architectures for waste heat recovery. Renew Sustain Energy Rev 2015;47:448–61.
[7] Branchini L, De Pascale A, Peretto A. Systematic comparison of ORC configurations by means of comprehensive performance indexes. Appl Therm Eng 2013;61: 129–40.
[8] Li J, Ge Z, Duan Y, Yang Z, Liu Q. Parametric optimization and thermodynamic performance comparison of single-pressure and dual-pressure evaporation organic Rankine cycles. Appl Energy 2018;217:409–21.
[9] Wang J, Yan Z, Wang M, Ma S, Dai Y. Thermodynamic analysis and optimization of an (organic Rankine cycle) ORC using low grade heat source. Energy 2013;49: 356–65.
[10] Liu B-T, Chien K-H, Wang C-C. Effect of working fluids on organic Rankine cycle for waste heat recovery. Energy 2004;29(8):1207–17.
[11] Hung TC, Wang SK, Kuo CH, Pei BS, Tsai KF. A study of organic working fluids on system efficiency of an ORC using low-grade energy sources. Energy 2010;35(3): 1403–11.
[12] Rayegan R, Tao YX. A procedure to select working fluids for solar Organic Rankine Cycles (ORCs). Renew Energy 2011;36(2):659–70.
[13] Long R, Bao YJ, Huang XM, Liu W. Exergy analysis and working fluid selection of organic Rankine cycle for low grade waste heat recovery. Energy 2014;73:475–83.
[14] Arjunan P, Gnana Muthu JH, Somanasari Radha SL, Suryan A. Selection of working fluids for solar organic Rankine cycle-a review. Int J Energy Res 2022;46(14): 20573–99.
[15] Tchanche BF, Lambrinos Gr, Frangoudakis A, Papadakis G. Low-grade heat conversion into power using organic Rankine cycles – a review of various applications. Renew Sustain Energy Rev 2011;15(8):3963–79.
[16] Loni R, Mahian O, Markides CN, Bellos E, le Roux WG, Kasaeian A, et al. A review of solar-driven organic Rankine cycles: recent challenges and future outlook. Renew Sustain Energy Rev 2021;150:111410.
[17] Gupta PR, Tiwari AK, Said Z. Solar organic Rankine cycle and its poly-generation applications – a review. Sustainable Energy Technol Assess 2022;49:101732.
[18] Kasaeian A, Mirjavadi K, Pourmoghadam P, Asgari Sima F, Amirhaeri Y, Borhani S, et al. Organic Rankine cycles powered by parabolic trough collectors: An overview. Sustainable Energy Technol Assess 2022;54:102847.
[19] Suleman F, Dincer I, Agelin-Chaab M. Development of an integrated renewable energy system for multigeneration. Energy 2014;78:196–204.
[20] Hassoun A, Dincer I. Analysis and performance assessment of a multigenerational system powered by organic Rankine Cycle for a net zero energy house. Appl Therm Eng 2015;76:25–36.
[21] Al-Sulaiman FA, Hamdullahpur F, Dincer I. Performance assessment of a novel system using parabolic trough solar collectors for combined cooling, heating, and power production. Renew Energy 2012;48:161–72.
[22] Bellos E, Tzivanidis C. Parametric analysis and optimization of a solar driven trigeneration system based on ORC and absorption heat pump. J Clean Prod 2017; 16110:493–509.
[23] García-Domínguez J, Marcos JD. Thermodynamic analysis and systematic comparison of solar-heated trigeneration systems based on ORC and absorption heat pump. Energies 2021;14:4770.
[24] Al-Sulaiman FA, Dincer I, Hamdullahpur F. Exergy modeling of a new solar driven trigeneration system. Sol Energy 2011;85(9):2228–43.
[25] Karellas S, Braimakis K. Energy–exergy analysis and economic investigation of a cogeneration and trigeneration ORC–VCC hybrid system utilizing biomass fuel and solar power. Energ Conver Manage 2016;107:103–13.
[26] Eisavi B, Khalilarya S, Chitsaz A, Rosen MA. Thermodynamic analysis of a novel combined cooling, heating and power system driven by solar energy. Appl Therm Eng 2018;129:1219–29.
[27] Khaliq A, Mokheimer EMA, Yaqub M. Thermodynamic investigations on a novel solar powered trigeneration energy system. Energy Conversion Management 2019; 188:398–413.
[28] Haghghi MA, Pesteei SM, Chitsaz A, Hosseinpour J. Thermodynamic investigation of a new combined cooling, heating, and power (CCHP) system driven by parabolic trough solar collectors (PTSCs): a case study. Appl Therm Eng 2019;163:114–329.
[29] Jafary S, Khalilarya S, Shawabkeh A, Wae-hayee M, Hashemian M. A complete energetic and exergetic analysis of a solar powered trigeneration system with two novel organic Rankine cycle (ORC) configurations. J Clean Prod 2021;281:124552.
[30] Aghaziarati Z, Aghdam AH. Thermoeconomic analysis of a novel combined cooling, heating and power system based on solar organic Rankine cycle and cascade refrigeration cycle. Renew Energy 2021;164:1267–83.
[31] Rosen MA, Dincer I. Effect of varying dead-state properties on energy and exergy analyses of thermal systems. Int J Therm Sci 2004;43(2):121–33.
[32] Blanco-Marigorta AM, Marcos JD. Key issues on the exergetic analysis of H_2O/LiBr absorption cooling systems. Case Studies in Thermal Engineering 2021;28:101568.
[33] Lazzaretto A, Tsatsaronis G. Speco: a systematic and general methodology for calculating efficiencies and costs in thermal systems. Energy 2006;31(8-9): 1257–89.
[34] Tzivanidis C, Bellos E, Antonopoulos KA. Energetic and financial investigation of a stand-alone solar-thermal Organic Rankine Cycle power plant. Energ Conver Manage 2016;126:421–33.
[35] Maraver D, Sin A, Sebastián F, Royo J. Environmental assessment of CCHP (combined cooling heating and power) systems based on biomass combustion in comparison to conventional generation. Energy 2013;57:17–23.
[36] Delgado-Torres AM, García-Rodríguez L. Comparison of solar technologies for driving a desalination system by means of an organic Rankine cycle. Desalination 2007;216(1-3):276–91.
[37] Tzivanidis C, Bellos E. A comparative study of solar-driven trigeneration systems for the building sector. Energies 2020;13:2074.
[38] Lemmon EW, Span R. Short fundamental equations of state for 20 industrial fluids. J Chem Eng Data 2006;51(3):785–850.
[39] Soltigua™. PTMx Parabolic Trough, https://www.soltigua.com/download/ptmx-brochure/ (Accessed 13 March 2023).
[40] Forristall R. Heat Transfer Analysis and Modeling of a Parabolic Trough Solar Receiver Implemented in Engineering Equation Solver. National Renewable Energy Laboratory; 2003.
[41] Therminol 66 Technical Bulletin, Heat transfer fluids by Eastman company, https://www.eastman.com/Literature_Center/T/TF8695.pdf#_ga=2.237448448.1080173255.1678742182-1577750596.1678742182 (Accessed 13 March 2023).
[42] Liao X., Garland P., Radermacher R., The modeling of air-cooled absorption chiller integration in CHP system, ASME International Mechanical Engineering Congress and Exposition IMECE2004-60308, 2004.
[43] Bakhtiari B, Fradette L, Legros R, Paris J. A model for analysis and design of H_2O–LiBr absorption heat pumps. Energ Conver Manage 2011;52(2):1439–48.
[44] Marcos JD, Izquierdo M, Palacios E. New method for COP optimization in water- and air-cooled single and double effect LiBr–water absorption machines. Int J Refrig 2011;34(6):1348–59.
[45] Evola G, Le Pierrès N, Boudehenn F, Papillon P. Proposal and validation of a model for the dynamic simulation of a solar-assisted single-stage LiBr/water absorption chiller. Int J Refrig 2013;36(3):1015–28.
[46] Herold KE, Radermacher R, Sanford AK. Absorption Chillers and Heat Pumps. second ed. Taylor & Francis, London: CRC Press; 2016.
[47] Cengel AY, Boles AM. Thermodynamics: An Engineering Approach. New York: McGraw-Hill; 1994.
[48] Dincer I, Midilli A, Kucuk H, editors. Progress in Exergy, Energy, and the Environment. Cham: Springer International Publishing; 2014.
[49] Hatsopoulous G, Keenan J. Principles of General Thermodynamics. New York: Wiley; 1965.

[50] Ahrendts J. Die Exergie Chemisch Reaktionsfähiger Systeme, Düsseldorf. Germany: VDI-Verlag; 1977.
[51] Dincer I., Rosen M.A., Chapter 2 - Exergy and Energy Analyses. Exergy (Second Edition), p.21-30, 2013b.
[52] Alpuche MG, Heard C, Best R, Rojas J. Exergy analysis of air cooling systems in buildings in hot humid climates. Appl Therm Eng 2005;25:507–17.
[53] Angelotti A., Caputo P., The exergy approach for the evaluation of heating and cooling technologies; first results comparing steady-state and dynamic simulations, Proceedings of the 2nd PALENC and 28th AIVC Conference 2007, vol. I, p. 59-64.
[54] Torio H, Schmidt D. Exergetic assessment and contribution of solar energy systems to the energy performance of buildings. Proceedings of the Nordic Symposium of Building Physics 2008;2:637–44.
[55] Gaggioli RA. The dead state. Int J Thermodyn 2012;15:191–9.
[56] Viswanathan VK, Rattner AS, Determan MD, Garimella S. Dynamic model for small-capacity ammonia-water absorption chiller. HVAC&R Research 2013;19:865–81.
[57] Petela R. Exergy of undiluted thermal radiation. Sol Energy 2013;74:469–88.
[58] Tsatsaronis G. Thermoeconomic analysis and optimization of energy systems. Prog Energy Combust Sci 1993;19:227–57.
[59] Dudley V, Kolb G, Sloan M, Kearney D. SEGS LS2 solar collector—Test results. of Sandia National Laboratories; 1994. Report No. SANDIA94-1884 Report.
[60] Koehler WJ, Ibele WE, Soltes J, Winter ER. Availability simulation of a lithium bromide absorption heat pump. Heat Recovery Syst CHP 1988;8:157–71.
[61] Palacios-Bereche R, Gonzales R, Nebra SA. Exergy calculation of lithium bromide–water solution and its application in the exergetic evaluation of absorption refrigeration systems LiBr-H2O. Int J Energy Res 2012;36:166–81.
[62] Avanessian T, Ameri M. Energy, exergy, and economic analysis of single and double effect LiBr–H2O absorption chillers. Energ Buildings 2014;73:26–36.
[63] Kim IY, de Weck OL. Adaptive weighted-sum method for bi-objective optimization: Pareto front generation. Struct Multidiscip Optim 2005;29:149–58.
[64] Zare V, Mahmoudi SMS, Yari M, Amidpour M. Thermoeconomic analysis and optimization of an ammonia-water power/cooling cogeneration cycle. Energy 2012;47:271–83.